Development and experimental investigation of a multi-ejector expansion work recovery pack for R744 vapour compression units

Krzysztof Banasiak [a] *, Armin Hafner [a], Ekaterini E. Kriezi [b], Kenneth B. Madsen [b], Michael Birkelund [b], Kristian Fredslund [b], Rickard Olsson [b]

[a] SINTEF Energy Research, Kolbjørn Hejes v. 1D, Trondheim, 7465, Norway

[b] DANFOSS A/S, Albuen 29, DK-6000 Kolding, Denmark

Abstract

A multi-ejector expansion pack, intended as a substitute for a standard high-pressure electronic expansion valve (HPV), was designed, manufactured and experimentally investigated. Four different ejector cartridges were sized to enable a discrete opening characteristic with a binary profile for a parallel-compression R744 system. The system is rated for 70 kW at a 35 °C gas cooler outlet temperature and a -3 °C evaporation temperature. High values of ejector efficiency, exceeding 0.3 over a broad operation range, were recorded for all four of the cartridges tested under vapour compression conditions. The applicability of the multi-ejector pack as a main flashing device was verified experimentally. Similar profiles of the discharge pressure control error were recorded for both alternative options: expansion purely in the HPV vs. HPV-assisted expansion in the multi-ejector pack.

Keywords: multi-ejector, expansion work recovery, R744, discharge pressure control

Nomenclature

A	coefficient in Eq. (1),	$m^4\ kg^{-1}\ s^{-1}$

* Corresponding author. Tel.: +47 73597200; fax: +47 73592889.
E-mail address: krzysztof.banasiak@sintef.no (K. Banasiak).

B	coefficient in Eq. (1), m s^{-1}
C	coefficient in Eq. (1), kg m^{-2} s^{-1}
D	coefficient in Eq. (1), kg m^{-2} s^{-1}
d	diameter, m
E	coefficient in Eq. (1), kg m^{-2} s^{-1}
K_i	dimensionless parameters in Eq. (2) and Eq. (3)
$k_{i,1}$	coefficient in Eq. (3), m^6 kg^2
$k_{i,2}$	coefficient in Eq. (3), m^3 kg
$k_{i,3}...k_{i,6}$	dimensionless coefficients in Eq. (3)
$\dot{m}$	mass flow rate, kg s^{-1}
p	pressure, Pa

Greek symbols

π	Ludolphian number, $\pi = 3.141593\ldots$
ρ	density, kg m^{-3}

Abbreviations

FC	frequency controller
GC	gas cooler
HPV	high-pressure valve
IHX	internal heat exchanger
LEJ	liquid ejector
LR	liquid receiver
LS	liquid separator
LT	low-temperature compressor
LTE	low-temperature evaporator

MT	medium-temperature compressor
MTE	medium-temperature evaporator
VEJ	vapour ejector

Subscripts

app	approximated value
cr	parameter in the critical point
DIF	diffuser
in	inlet value
meas	measured value
MN	motive nozzle
out	outlet value
SN	suction nozzle
th	parameter at the nozzle throat

1. Introduction

Application of ejectors in R744 (CO_2) refrigeration and heat pump systems is one of the best methods to reduce the throttling loss and increase the system energy efficiency. Two-phase ejectors partially utilize the expansion work available when the high-pressure refrigerant is expanded in a motive nozzle inside an ejector. This reduces the compressor pressure ratio and the required compression work. The energy saving effect was experimentally verified by laboratory tests for the single-ejector system architecture, e.g., Elbel (2011), Nakagawa et al. (2011b), Banasiak et al. (2012) and Liu et al. (2012). The registered improvement in the coefficient of performance (COP) ranged from 8% to 60%, depending on the system architecture and operating conditions analysed.

Consequently, commercial systems equipped with ejector(s) can also achieve COP values higher than the values for the conventional R744 systems (booster assisted by parallel compression) and the HFC systems. Intensive system simulations and laboratory experiments showed that the COP of the commercial refrigeration systems equipped with a single ejector could be increased even by 20% at high ambient temperatures, as validated by Girotto (2012).

Because of the constraint of constant ejector geometry, the disadvantage of a single-geometry system is its poor ability to precisely control the discharge pressure and effectively recover expansion work simultaneously. Although the motive nozzle mass flow rate can be regulated by controlling the motive nozzle throat area, e.g., Liu et al. (2012), there has not been a reported attempt to simultaneously regulate the mixer/diffuser geometries, which is required to maintain high ejector efficiency over a broad operation range. To avoid the use of advanced mechanisms for controlling the motive nozzle capacity (reduced efficiency, high costs, lower reliability, etc.) and to ensure high energy performance independent of the operating conditions (with respect to both refrigeration load and ambient temperature), an alternative is a system equipped with a series of different constant-geometry ejectors assembled in parallel, operated together with a reduced-capacity expansion valve for precise adjustment of the discharge pressure.

The multiple-ejector concept was described and theoretically analysed in a paper by Hafner et al. (2014a), where dynamic modelling for supermarket refrigeration and heat recovery systems with multiple ejectors revealed that the multi-ejector system offers a significant increase in the COP for the cooling and heating modes. The COP increase is highly dependent on the system control strategy. Typical COP increases during the cooling mode of 17% in Athens, 16% in Frankfurt and 5% in Trondheim in the summer were simulated. In the winter, the typical COP increase was between 20% and 30%.

Use of the multi-ejector expansion work recovery system has not been realized in practice in commercial refrigeration. A proper design of a multi-ejector expansion work recovery pack for commercial heat, ventilation, air conditioning and refrigeration (HVAC&R) units requires detailed knowledge of the system architecture, installation load profile and climate data of the potential location. Therefore, the primary objective of this research was the development and experimental testing of a prototype multi-ejector expansion work recovery pack for R744 vapour compression units dedicated to covering refrigeration loads of a typical supermarket.

2. Design procedure

2.1 Vapour compression unit architecture and controlling strategy

The multi-ejector expansion work recovery system (Fig. 1) substitutes for a single high-pressure valve (HPV) used in conventional booster systems to reduce high pressures below a certain level (typically 40×10^5 Pa) before metering refrigerant to the individual cabinets/cold room evaporators (LTE and MTE). A series of vapour ejectors are assembled in parallel (from VEJ1 to VEJ4). The geometry of each ejector can be optimized for different operating conditions governed by variable ambient temperatures. Every ejector is individually controlled by a shut-off valve at the inlet to the motive nozzle and a check valve at the inlet to the suction nozzle. Thus, by controlling the number of ejectors in operation and maintaining the high side pressure level according to ambient temperature or load requirements, system operation at the maximized overall COP should be possible. Additionally, an auxiliary liquid ejector (LEJ) compresses the remaining liquid not vaporized in the evaporators, while benefitting from the advantages of wet evaporators (optimum use of the effective heat transfer

area, higher values of the heat transfer coefficient, simpler and cost-effective metering valves, etc.).

The medium-temperature compressors (MT) are either connected to the liquid receiver (LR) or to the liquid separator (LS) downstream from the ejectors. MT2 and MT3 can work in alternative modes whereas the frequency-controlled MT1 and MT4 are devoted to a specific operation mode, i.e., MT1 pumps out the return gas from the evaporators while MT4 pumps out the flash gas from the liquid separator. This architecture elevates the suction pressure in the medium-temperature evaporators much higher than a conventional R744 booster system, where all of the compressors are connected to the exits of the evaporators. The ejectors are applied to maintain a required pressure difference between the liquid separator and the liquid receiver for proper feeding of individual cabinets.

At low and moderate ambient temperatures, the optimum high side pressure is low, i.e., a subcritical mode of the R744 system is selected. In this case, the pressure lift capability of the ejectors is reduced because less work can be recovered from the condensate expansion. Therefore, the number of compressors connected to the liquid receiver increases. This reduces the entrainment ratio of the ejectors, which supports the ejectors in operation to maintain the necessary pressure lift.

Proper oil management can be performed both on the discharge side (before the gas cooler) and on the suction side (inside the liquid separator) by the pressure lift invoked by the ejectors.

2.2 Boundary conditions for the multi-ejector pack

To determine the operational envelope for a sample multi-ejector pack, a mathematical model of the R744 refrigeration installation for a typical supermarket was created. A

calculation worksheet supplied with the REFPROP 9.1 library for the R744 thermal and transport properties was used and a series of system simulations was carried out by a non-linear equation solver. The mass and energy balances for the components of the refrigeration installation were formulated, accompanied by the definitions of isentropic, volumetric and mechanical efficiency for the compressors. The ejectors were modelled by the approximation function for the primary flow invoked in a particular geometry under given operating conditions based on the results of 1D simulations performed by the previously developed and validated models, Banasiak and Hafner (2011), Banasiak and Hafner (2013).

The analysed system layout was defined according to Fig. 1, i.e., a rack of six compressors (2 LT and 4 MT) working together with a series of four vapour ejectors and one liquid ejector connected in parallel. The multi-ejector pack, where the nominal openings (motive nozzle throat diameter) of the vapour ejectors were increasing in binary order (1:2:4:8, which gives discrete, sixteen-point opening characteristics), was utilised as the primary expansion device. The high-pressure valve was utilised merely for control purposes, i.e., to precisely adjust the discharge pressure to the maximum system COP value for the given operating conditions. The simulations were performed with the following constraints:

- MT evaporation temperature equal to –3 °C, outlet quality equal to 90%.
- LT evaporation temperature equal to –30 °C, outlet superheat equal to 8 K.
- Discharge pressure as a function of the gas cooler outlet temperature: corresponding to 5 K of subcooling in the subcritical conditions and optimised for the maximum COP in the transcritical conditions.
- Maximum pressure in the liquid separator: 40×10^5 Pa.
- Pressure difference between the liquid separator and the liquid receiver: optimised (with the 4×10^5 Pa technical minimum due to the necessity of proper feeding to the evaporator lines).

- Nominal capacity of the MT cabinets: 70 kW.
- Nominal capacity of the LT cabinets: 23 kW.
- Nominal gas cooler outlet temperature: 35 °C.
- Volumetric, isentropic and mechanical efficiency of compressors dependent on rotational speed and pressure ratio according to the approximation functions presented by Bou Lawz Ksayer (2007).
- The liquid ejector motive nozzle modelled as an adjustable nozzle providing suitable driving flow to evacuate all of the condensate from the liquid receiver to the liquid separator during continuous operation.
- The ejectors working with constant efficiency, equal to 25% for the vapour ejector and 15% for the liquid ejector, where the ejector efficiency was defined according to Elbel and Hrnjak (2008).
- The minimum feasible throat diameter (due to manufacturing limits/requirements) of the motive nozzle equal to 1 mm.

The changeability of operating conditions was represented by variation in the gas cooler outlet temperature, set to 15 °C, 25 °C and 35 °C. The set of operation conditions at full load obtained from the simulations for the three cases considered was gathered in Table 1.

2.3 Ejector sizing

The overall outline of the ejector flow channels applied (axisymmetric geometry with coaxially arranged motive nozzle, suction nozzle, mixer and diffuser, etc.) was explained in more detail in the authors' previous publications, Banasiak and Hafner (2011), and Banasiak et al. (2012).

To match the required mass flow rates specified in Table 1, a sizing procedure was applied based on the previously developed 1D model, Banasiak and Hafner (2011). Over the course of multiple optimization simulations (where the mass entrainment ratio was maximized, when averaged over the three levels of the gas cooler outlet temperature) the initial set of geometries was proposed for the VEJ group. The initial set consisted of four ejectors, and the LEJ group consisted of two ejectors (due to high changeability of the motive nozzle mass flow rate for the LEJ, it was decided to split the overall duty into two LEJ geometries). However, to reduce the manufacturing cost, the dedicated liquid ejectors were replaced by the vapour ejectors, VEJ1 for LEJ1 and VEJ2 for LEJ2 (see Table 2). The primary rationale was that the main dimensioning parameter, the motive nozzle throat diameter, was identical for each original-substitute pair, while the operating hours predicted for the auxiliary liquid ejectors (working only periodically in practice) were substantially reduced.

Modular design of the multi-ejector pack was applied, where individual ejector cartridges were placed into a monoblock casing, instead of a set of separate ejectors. This modification enabled very compact design (crucial for the units dedicated to supermarket applications) and easier integration of the necessary accompanying automation and controlling components. However, this modification prevented individual measurements of each particular cartridge during simultaneous operation of the entire pack of parallel ejectors. Therefore, the ejector performance mapping was carried out individually for each cartridge in the course of separated runs.

3. Test facility layout

The laboratory tests of the multi-ejector pack were performed at the facility designed and assembled at SINTEF Energy Research (Fig. 2). The facility consisted of the two main circuits: a refrigerant loop and a glycol loop where the latter was integrated to simultaneously serve as both heat sink and heat supply. Additionally, two auxiliary networks were utilized, namely the cooling water network, providing the cooling medium of the inlet to maintain a temperature between 15 °C and 18 °C, and the ice water network, facilitating the maintenance of the cooling medium at a temperature down to 2 °C.

The multi-ejector pack was operated in parallel with a high-pressure expansion valve that ensured precise high pressure control during the operation. The motive nozzle manifold was connected to the high pressure side through a separate mass flow meter enabling monitoring of the motive mass flow through the ejector block. Both liquid and vapour suction manifolds were connected to the liquid receiver located downstream from the evaporators via individual mass flow meters. The ejectors discharged into a liquid separator, separating the vapour from the liquid, dividing the refrigerant stream into two parts. The vapour was compressed by the parallel compressors while the liquid was circulated through the evaporator before entering the liquid receiver. Depending on the operational mode, the pressure level in the liquid receiver was determined by the vacuum pressure of the base-load compressor, the opening degree of the flash valve, or the ejector capacity.

The refrigerant loop consisted of the following components:

- three piston-type R744 compressors (Dorin CD380H and CD1000H as the parallel machines, and Dorin CD1400H as the base-load machine),

- four brazed plate heat exchangers (two Kaori K095C-30C-NP8M as the second-stage gas cooler and peak-load evaporator, SWEP B18Hx100 as the first-stage gas cooler, and SWEP B16DWHx100 as the base-load evaporator),
- four electronic expansion valves (two Danfoss CCMT8 as the flash valve and the high-pressure valve, two Danfoss CCM20 as the metering valves at evaporators),
- two pressure tanks with liquid level indication (two 50-litre vessels for liquid separator and liquid receiver, two Danfoss AKS 4100 level sensors),
- an integrated multi-ejector pack (a prototype manufactured by Danfoss, containing ejector cartridges and auxiliary automation components, i.e., solenoid valves for supplying the motive nozzles with high-pressure refrigerant as well check valves for preventing back flow).

The data acquisition system was equipped with the Danfoss AKS 21 A PT1000 temperature sensors (calibrated resistance thermometers), Danfoss AKS 2050 gauge pressure sensors (calibrated piezoelectric transmitters), and RHEONIK RHM06 (refrigerant circuit) and RHEONIK RHM15 (glycol circuit) mass flow meters (calibrated Coriolis type). The mean values of the measurement uncertainties registered, including both the sensor accuracies and the time-averaged deviations from steady state, were as follows: ±0.6 K for the temperature measurements, $\pm 2.5 \times 10^{4}$ Pa for the pressure measurements, and $\pm 0.5 \times 10^{-3}$ kg s^{-1} for the mass flow rate measurements.

4. Experimental tests

The campaign of experimental tests consisted of performance mapping for individual ejector cartridges and trial runs of the multi-ejector pack operated as the main expansion device maintaining the required discharge pressure.

4.1 Ejector performance mapping

Performance of an ejector, expressed by the primary stream mass flow rate and secondary stream mass flow rate, is determined by five independent variables: motive nozzle inlet pressure and density, suction nozzle inlet pressure and density, and outlet pressure. This sets the number of physically possible boundary conditions beyond a manageable level when experimentally mapping performance curves. Therefore, to limit the number of tests required while maintaining high recorded data resolution, the range of boundary conditions for the investigated ejector cartridges was structured to cover just the most common configurations of operating points enforced by a controller of a modern R744 parallel-compression unit for supermarkets, Hafner et al. (2014b), namely:

- Several levels of the heat sink temperature were tested where the motive nozzle inlet conditions were defined by (i) slight subcooling (up to 5 K) for subcritical operation and (ii) discharge pressure optimized according to the maximum system COP for transcritical operation. The area of high pressure and low temperature (e.g., 85×10^5 Pa, 15 °C) was also investigated to simulate the heat recovery operation mode.
- The suction nozzle inlet conditions were determined by two levels of evaporation pressure, i.e., 28×10^5 Pa and 32×10^5 Pa; saturated liquid conditions for the LEJ group and superheated (by ca. 10 K) vapour conditions were maintained for the VEJ group.

- Several levels of pressure lift between 4×10^5 Pa and 7×10^5 Pa were investigated for each set of the inlet conditions.

To improve the mapping resolution and produce a more detailed representation of the ejector performance for at least one geometry, the number of investigation points for VEJ1 was increased significantly to 400.

4.1.1 Motive nozzle mass flow rate

The recorded values for all of the geometries were presented in a form of two-dimensional, motive-inlet-dependent profiles (Fig. 3a to 3d) due to the supersonic flow conditions at the motive nozzle outlet, for which neither suction pressure nor pressure lift influences the motive nozzle mass flow rate. The registered profiles were clearly dependent on the inlet density and inlet pressure, where the highest mass flow rate values were recorded for the heat recovery operation mode while the lowest occurred in the vicinity of the switching point between the subcritical and supercritical operation modes.

The motive nozzle mass flow rate profiles are expressed as functions of the following structure,

$$\dot{m}_{\mathrm{MN}} = \pi/4\, d_{\mathrm{th}}^{\,2}\left[A\rho_{\mathrm{MN,in}}^{\,2} + B\rho_{\mathrm{MN,in}} + C\left(p_{\mathrm{MN,in}}/p_{\mathrm{cr}}\right)^2 + D\,p_{\mathrm{MN,in}}/p_{\mathrm{cr}} + E\right] \qquad (1)$$

where A, B, C, D and E are coefficients adjusted individually for a particular cartridge. For example, based on the increased-resolution area investigated for VEJ1, $A = 1.71938\times10^{-1}$ m^4 kg^{-1} s^{-1}, $B = -6.06326\times10^{1}$ m s^{-1}, $C = 4.55787\times10^{3}$ kg m^{-2} s^{-1}, $D = 4.98027\times10^{4}$ kg m^{-2} s^{-1}, and

$E = -5.46798 \times 10^4$ kg m^{-2} s^{-1}. The corresponding profile of the registered relative errors, defined as $\frac{\dot{m}_{\mathrm{MN,app}} - \dot{m}_{\mathrm{MN,meas}}}{\dot{m}_{\mathrm{MN,meas}}}$, lies between –6.95% and +5.56% (see Fig. 4), which reveals reasonable accuracy of the proposed approximation. The application range for the approximation functions should be strictly limited to the area covered by the experimental work performed for individual cartridges.

4.1.2 Suction nozzle mass flow rate, entrainment ratio, and ejector efficiency – vapour compression

In contrast to the motive nozzle, the suction nozzle mass flow rate is a function of more than two independent parameters. Therefore, it is not possible to graphically present representative performance maps for the suction nozzle mass flow rate unless three of the five degrees of freedom are held constant. The same conclusion applies to derivative parameters such as entrainment ratio and ejector efficiency.

A number of the five degrees of freedom reportedly have less significant effect than others and can be neglected. Namely, moderate superheating of the suction stream also causes a moderate reduction in density when compared to the saturation conditions. Therefore, it may be presumed that within a limited range (from 0 K to 10 K), the influence of superheating on the ejector performance will be barely measurable. For the purpose of presentation, if the influence of the suction/outlet conditions becomes expressed solely by the pressure ratio, i.e., the ratio of the ejector outlet pressure to the suction pressure, then individual quasi-maps for ejector suction performance may be generated either explicitly for the suction nozzle mass flow rate or for any derivatives, e.g., ejector efficiency (Fig. 5a to 5d).

The registered profiles, particularly the high-resolution efficiency map for VEJ1, prove effective vapour compression over a broad range of operating conditions. According to

the data presented in Fig. 5a, the region where the ejector efficiency is equal to at least 0.3 may be found from ca. 70×10^5 Pa to ca. 95×10^5 Pa and from ca. 25 °C to ca. 35 °C for the motive nozzle inlet conditions, which constitutes a substantial part of the operational area. At the same time, clear dependence between the maximum performance pressure ratio and the motive nozzle inlet conditions are observed. All of the points characterized by ejector efficiency greater than or equal to 0.3 recorded at the inlet pressure higher than 90×10^5 Pa were reached with a substantial pressure ratio, ranging from 1.22 to 1.31. Conversely, points with an ejector efficiency greater than or equal to 0.3 recorded at inlet pressures lower than 75×10^5 Pa were reached with a much lower pressure ratio that ranged between 1.15 – 1.18. Thus, the recorded profiles suggest that to utilize a given ejector geometry in the optimum way, one should adjust the floating pressure ratio (or pressure lift) according to the heat sink conditions in the gas cooler. It should be noted that each ejector cartridge may provide an individual performance map of unique features. Thus, by applying common boundary conditions to a series of parallel ejectors placed in operation, the overall system performance should be maximized because it is not possible to optimise individual ejector operations simultaneously.

It should be emphasised that the recorded levels of ejector efficiency for the four cartridges outperformed reported achievements to date. Namely, Elbel and Hrnjak (2008) registered values at or below 0.145, while Nakagawa et al. (2011a) reached values as high as ca. 0.22. Approximately the same maximum level, 0.22, was recorded by Lucas and Koehler (2012), while Xu et al. (2012) managed to reach efficiencies as high as 0.282. The highest efficiency values were reported by Banasiak et al. (2012), specifically up to 0.308. In the current research, the highest measured efficiency for VEJ1 was 0.330, 0.368 for VEJ2, 0.362 for VEJ3, and 0.336 for VEJ4, respectively.

The vapour compression performance of each ejector cartridge is expressed by functions of the following structure,

$$\dot{m}_{\mathrm{SN}} \Big/ \dot{m}_{\mathrm{MN}} = K_1 \left(p_{\mathrm{DIF,out}} \Big/ p_{\mathrm{SN,in}} \right)^2 + K_2 \, p_{\mathrm{DIF,out}} \Big/ p_{\mathrm{SN,in}} + K_3 \qquad (2)$$

with parameters $K_1 \ldots K_3$ defined as follows:

$$K_{\mathrm{i}} = \left[k_{\mathrm{i},1} \rho_{\mathrm{MN,in}}{}^2 + k_{\mathrm{i},2} \rho_{\mathrm{MN,in}} + k_{\mathrm{i},3} \left(p_{\mathrm{MN,in}} \Big/ p_{\mathrm{cr}} \right)^2 + k_{\mathrm{i},4} \, p_{\mathrm{MN,in}} \Big/ p_{\mathrm{cr}} \right] \left(k_{\mathrm{i},5} \, p_{\mathrm{SN,in}} \Big/ p_{\mathrm{cr}} + k_{\mathrm{i},6} \right) \qquad (3)$$

where coefficients $k_{\mathrm{i},1} \ldots k_{\mathrm{i},6}$ are adjusted individually for a particular cartridge. The values from the increased-resolution area investigated for VEJ1are shown in Table 3.

Because the registered entrainment ratio of VEJ1varied greatly from 0 to ca. 0.6, the relative expressions of the approximation errors were discarded. Because the relative values were approaching infinity for an entrainment ratio close to 0, giving a false indication of substantial inaccuracy, the absolute errors were calculated instead (see Fig. 6). It was verified that for 358 test points of the 400 points analysed for VEJ1, the absolute error was less than ±0.02, while for 397 points, the absolute error was less than ±0.04.

4.1.3 Suction nozzle mass flow rate, entrainment ratio, and ejector efficiency – liquid compression

Although the number of points investigated was limited, it is possible to measure the influence of pressure ratio on the ejector's performance (see Fig. 7). Namely, the higher the

motive nozzle inlet pressure, the higher the optimum pressure ratio. Nevertheless, the overall efficiency of the liquid compression level is much lower (ca. three times) than the efficiency of the vapour compression performed with the same cartridges. This indicates that the ejectors optimised for vapour compression perform relatively ineffectively during liquid pumping. Therefore, the ejectors in the liquid return section should be individually sized.

4.2 Test runs with the multi-ejector block as the main expansion device

After the ejector cartridges were verified individually, a series of test runs for the entire multi-ejector block was performed to prove its suitability as the primary component for regulating the discharge pressure in the system. Because of the non-optimized liquid ejector cartridges, the experiments were performed under the superheat conditions at the evaporator outlet(s). Wet-evaporator tests using the LEJ section are planned in the immediate future.

Because optimization of the controlling algorithms exceeds the scope of the paper, a simplified procedure was applied to regulate the discharge pressure. The requested configuration of ejectors in use at any given time was dependent on the opening degree of the accompanying HPV working in parallel. Each time the registered opening degree of the HPV rose to the 'step-up' level, the next point of higher capacity on the multi-ejector opening characteristics was applied by switching on/off the appropriate solenoid valves. Accordingly, every time the HPV opening degree sank to the 'step-down' level, the closest point of lower capacity for the multi-ejector block was selected. Thus, the applied controlling algorithm required neither additional sensor(s) nor advanced logic.

The recorded system performance for the HPV-assisted operation of the multi-ejector block was compared to the standard HPV operation. Two test cases were run, one verifying the system reaction for a quick jump in the load profile (Fig. 8), and the other verifying the

system response to a rapid change in ambient conditions (Fig. 9). Identical values of proportional gain and integration time for the HPV controller were used for both expansion modes. The key system settings for the test conditions are shown in Table 4.

The system's response to a shock increment in the load profile was relatively similar for both operation modes. The same profiles of the heat source temperature (Fig. 8a) resulted in profiles of discharge pressure control errors of comparable magnitudes and trends (Fig. 8c), though slightly different in shape. Unlike in the pure HPV mode, the discrete feature of the multi-ejector opening characteristics invoked a fluctuation of the control discrepancy, which increased its integrated values. The standard deviation of the discrepancy over the recorded test periods was 1.20×10^5 Pa compared to 0.75×10^5 Pa for the pure HPV mode. However, the stepwise-occurring control gaps invoked by stepping up/down were not large (less than 2×10^5 Pa at their peaks) and were alleviated over time by the opening/closing HPV compensating for a too large or too small overall opening of the multi-ejector block. Additionally, the magnitude and frequency of the resulting oscillations in control error can be influenced by settings of the regulator parameters, so further optimization of the controlling algorithm is possible.

The system's response to a shock increment in the ambient conditions again proved to be similar in terms of magnitude and trend for the control error profile in both controlling modes (Fig. 9c) despite different profiles of the HPV opening degree (Fig. 9b). The standard deviation of the control error over the recorded period was 1.11×10^5 Pa for the HPV mode and 0.96×10^5 Pa for the HPV-assisted mode.

In general, a relatively flat shape of the COP curve (expressed as a function of the discharge pressure) shall prevent significant penalty in the integrated value of the system energy performance caused by an aggregated control gap resulting from the discrete opening characteristics of the multi-ejector block. Furthermore, the overall system performance will be

enhanced by the effects of the expansion work recovery. The percentage of the mass flow rate expanded through the multi-ejector block registered during these tests was high and varied between 84% and 96%, even though the controlling algorithm was not optimized. In the immediate future, it is planned to equip the test facility with individual power meters for each compressor and verify the expected COP gain experimentally.

5. Conclusions

The proposed concept of replacing a standard high-pressure expansion valve with a block of properly designed parallel ejectors for maintaining the discharge pressure in R744 parallel-compression systems was successfully verified under laboratory conditions. It was proven that the refrigeration system upgraded with the multi-ejector block fully retains its dynamic operational characteristics, and precise discharge pressure adaptations according to the variable load and ambient conditions are possible, even with the use of a simplified controlling strategy.

Based on the high values of ejector efficiency recorded (broad areas of efficiency higher than 0.3 for the four vapour-compression cartridges), the system overall energy performance can be substantially improved when utilising the multi-ejector block as a main flashing device because of the expansion work recovery invoked and consequent transfer of the load from the base-load compressors group to the parallel compressors group.

To use the wet-evaporator controlling strategy, potentially providing the benefits of elevation of the requested evaporation temperature and the enhanced heat transfer mechanism, reliable high-efficiency liquid ejectors must be developed and incorporated into the multi-ejector pack, ensuring effective liquid removal from the liquid receiver under all operating conditions.

A new test campaign is planned to verify the reliability of the developed multi-ejector block and identify any potential wear mechanisms that may shorten the life of block components (solenoid valves, check valves, ejector flow passages, etc.). Based on the results gained, the controlling logic will be optimized and the electronic hardware will be adapted accordingly.

Additionally, two independent field test campaigns are planned for the integrated multi-ejector-equipped R744 installations covering the needs of the supermarket facilities (heating, cooling, chilling and air conditioning) where detailed, year-round COP recordings will be gathered for the two alternative flashing modes (pure HPV vs. HPV-assisted multi-ejector) to estimate actual feasible COP gains.

References

Banasiak, K., Hafner, A., 2011, 1D Computational model of a two-phase R744 ejector for expansion work recovery, International Journal of Thermal Sciences 50, 2235–2247.

Banasiak, K., Hafner, A., Andresen, T., 2012. Experimental and numerical investigation of the influence of the two-phase ejector geometry on the performance of the R744 heat pump. Int. J. Refrigeration 35, 1617–1625.

Banasiak, K., Hafner, A., 2013, Mathematical modelling of supersonic two-phase R744 flows through converging-diverging nozzles: the effects of phase transition models, Applied Thermal Engineering 51, 635–643.

Bou Lawz Ksayer E., Etude et conception de systemes a efficacite energetique amelioree fonctionnant au CO_2 comme fluide frigorigene, PhD dissertation, Paris 2007.

Elbel, S., Hrnjak, P., 2008. Experimental validation of a prototype ejector designed to reduce throttling losses encountered in transcritical R744 system operation. Int. J. Refrigeration 31, 411–422.

Elbel, S., 2011. Historical and present developments of ejector refrigeration systems with emphasis on transcritical carbon dioxide air-conditioning applications. Int. J. Refrigeration 34, 1545–1561.

Girotto S., 2012. Efficiency improvement in commercial refrigeration for warmer climates with CO_2, Proceedings from the ATMOsphere Europe 2012, 5-7.11.2012, Brussels.

Hafner, A., Försterling, S., Banasiak, K., 2014, Multi-Ejector Concept for R-744 Supermarket Refrigeration, Int. J. Refrigeration 43, 1–13.

Hafner, A., Schönenberger, J., Banasiak, K., Girotto, S., 2014, R744 ejector supported parallel vapour compression system, Refrigeration Science and Technology, 3rd IIR International Conference on Sustainability and the Cold Chain, 134–141.

Liu, F., Li, Y., Groll, EA, 2012, Performance enhancement of CO_2 air conditioner with a controllable ejector, Int. J. Refrigeration 35, 1604–1616.

Lucas, C., Koehler, J., 2012. Experimental investigation of the COP improvement of a refrigeration cycle by use of an ejector. Int. J. Refrigeration 35, 1595–1603.

Nakagawa, M., Marasigan, A.R., Matsukawa, T., 2011, Experimental analysis on the effect of internal heat exchanger in transcritical CO_2 refrigeration cycle with two-phase ejector, Int. J. Ref. 34, 1577–1586.

Nakagawa, M., Marasigan, A.R., Matsukawa, T., Kurashina, A., 2011, Experimental investigation on the effect of mixing length on the performance of two-phase ejector for CO_2 refrigeration cycle with and without heat exchanger, Int. J. Refrigeration 34, 1604–1613.

Xu, X.X., Chen, G.M., Tang, L.M., Zhu, Z.J., 2012, Experimental investigation on performance of transcritical CO_2 heat pump system with ejector under optimum high-side pressure, Energy 44, 870–877.

Tables

Motive nozzle inlet		Suction nozzle inlet		Required pressure lift, Pa	Total required mass flow rate expanded through motive nozzles, kg s^{-1}	
Pressure, Pa	Temperature, °C	Pressure, Pa	Quality LEJ/VEJ, -		LEJ	VEJs
93.9×10^5	35	32×10^5	0/1	6.1×10^5	0.0109	0.723
72.1×10^5	25	32×10^5	0/1	4.9×10^5	0.0152	0.590
57.3×10^5	15	32×10^5	0/1	4.0×10^5	0.0255	0.484

Table 1. The simulated set of boundary conditions for the multi-ejector expansion work recovery pack.

Parameter name, unit	Geometry					
	VEJ1	VEJ2	VEJ3	VEJ4	LEJ1	LEJ2
Motive nozzle inlet diameter, 10^{-3} m	3.8	3.8	3.8	3.8	3.8	3.8
Motive nozzle throat diameter, 10^{-3} m	1.00	1.41	2.00	2.83	1.00	1.41
Motive nozzle outlet diameter, 10^{-3} m	1.12	1.58	2.24	3.16	1.12	1.58
Motive nozzle converging angle, °	30	30	30	30	30	30
Motive nozzle diverging angle, °	2	2	2	2	2	2
Diffuser outlet diameter, 10^{-3} m	7.3	8.4	10.3	13.1	7.3	8.4
Diffuser angle, °	5	5	5	5	5	5

Table 2. The primary geometry parameters of the multi-ejector pack.

Coefficient K_i	$k_{i,1}$, $m^6\ kg^2$	$k_{i,2}$, $m^3\ kg$	$k_{i,3}$, –	$k_{i,4}$, –	$k_{i,5}$, –	$k_{i,6}$, –
i = 1	-9.86734×10^{-5}	7.39056×10^{-2}	-1.45771×10	1.38768×10	5.04109×10^{-1}	-1.20796×10^{-1}
i = 2	1.30593×10^{-4}	-1.11153×10^{-1}	8.90401	–3.10430	1.48557	-3.22489×10^{-1}
i = 3	-1.59391×10^{-5}	1.34518×10^{-2}	–1.08935	8.42101×10^{-1}	8.50832	–1.45925

Table 3. Coefficients in Eq. (3) matched for VEJ1.

R744 circuit	
Evaporation temperature, °C	–5
Evaporator outlet superheat, K	10
Gas cooler outlet temperature (after 2nd stage), °C	25
Liquid separator pressure, 10^5 Pa	34
Glycol circuit	
Evaporator inlet temperature, °C	15
Evaporator circuit mass flow rate, kg s^{-1}	0.81

Table 4. Test settings for the system's response verification runs.

Figure captions

Fig. 1. Schematic representation of the novel multi-ejector pack for expansion work recovery in R744 refrigeration units for supermarkets. Standard components in the booster system are presented in black, and additional components of the energy recovery system are indicated in red.

Fig. 2. Schematics of the multi-ejector test facility, (a) R744 circuit and (b) glycol circuit. Instrumentation signatures: t – temperature sensor, p – absolute pressure sensor, m – mass flow rate meter.

Fig. 3. Motive nozzle mass flow rate as a function of the motive nozzle inlet conditions for VEJ1 (a), VEJ2 (b), VEJ3 (c), and VEJ4 (d).

Fig. 4. Relative errors between the approximation function given by Eq. (1) and measured values of the motive nozzle mass flow rate for VEJ1.

Fig. 5. Ejector efficiency as defined by Elbel and Hrnjak (2008) as a function of the motive nozzle inlet conditions and pressure ratios for VEJ1 (a), VEJ2 (b), VEJ3 (c), and VEJ4 (d). The average measurement uncertainties for ejector efficiency are ±0.008 (a), ±0.004 (b), ±0.008 (c), ±0.006 (d), respectively.

Fig. 6. Absolute errors between the approximation function given by Eq. (2) and measured values of the entrainment ratio for VEJ1.

Fig. 7. Ejector efficiency as defined by Elbel and Hrnjak (2008) as a function of the motive nozzle inlet conditions and pressure ratios for LEJ1 (spheres) and LEJ2 (cubes). The average measurement uncertainties for ejector efficiency are ±0.002 for both cartridges.

Fig. 8. System's response to a rapid change in load for the HPV operation mode (red profiles) and HPV-assisted multi-ejector operation mode (green profiles). Evaporator inlet temperature in the glycol circuit (a), opening degree of HPV and indication of the ejector cartridges in use (b), and deviation between the actual value and set-point value for the discharge pressure (c).

Fig. 9. System's response to a rapid change in ambient conditions for the HPV operation mode (red profiles) and HPV-assisted multi-ejector operation mode (green profiles). Gas cooler outlet temperature (a), opening degree of HPV and indication of the ejector cartridges in use (b), and deviation between the actual value and set-point value for the discharge pressure (c).

Figure_1

Click here to download high resolution image

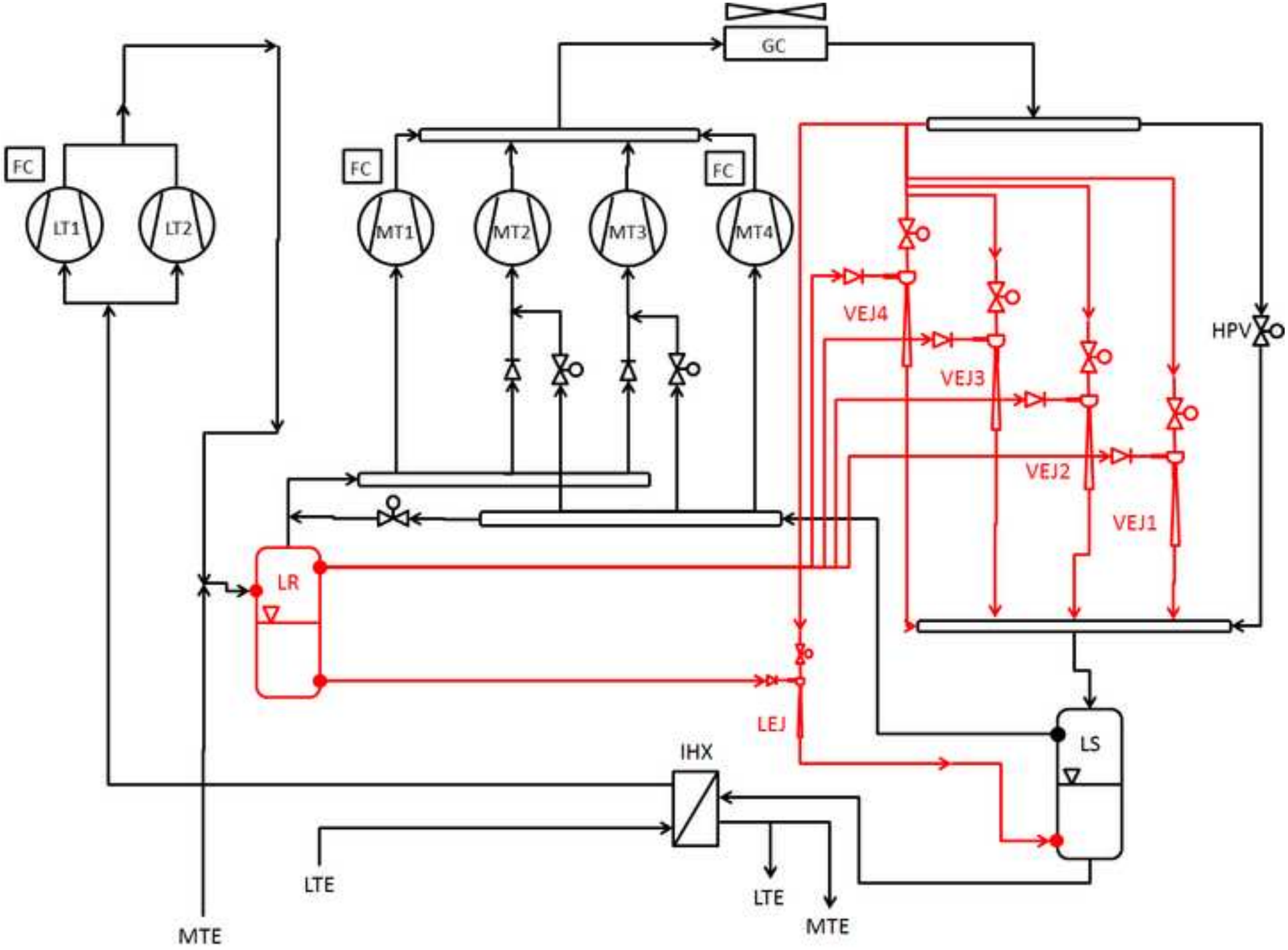

Figure_2a

Click here to download high resolution image

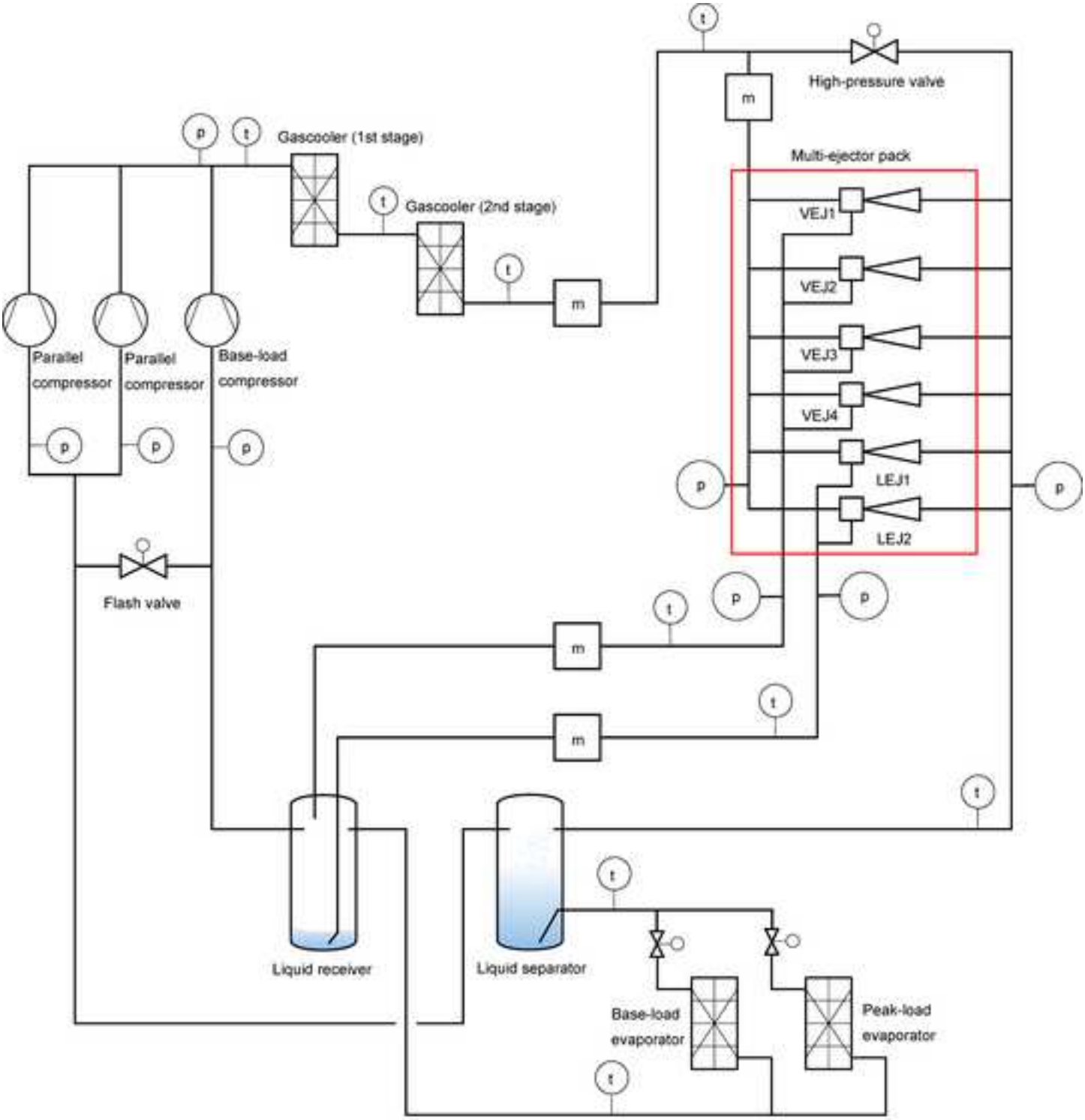

Figure_2b

Click here to download high resolution image

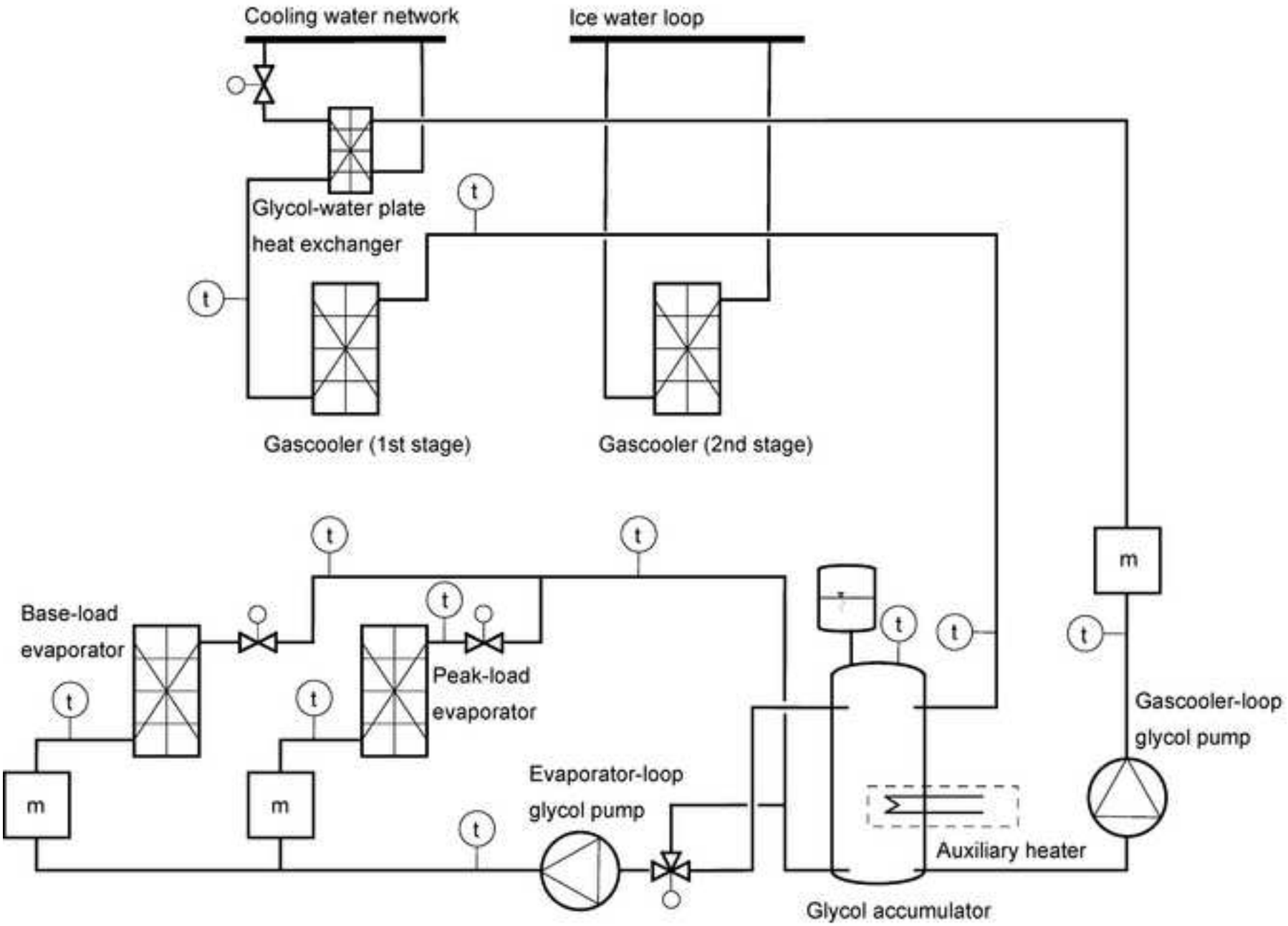

Figure_3a

Click here to download high resolution image

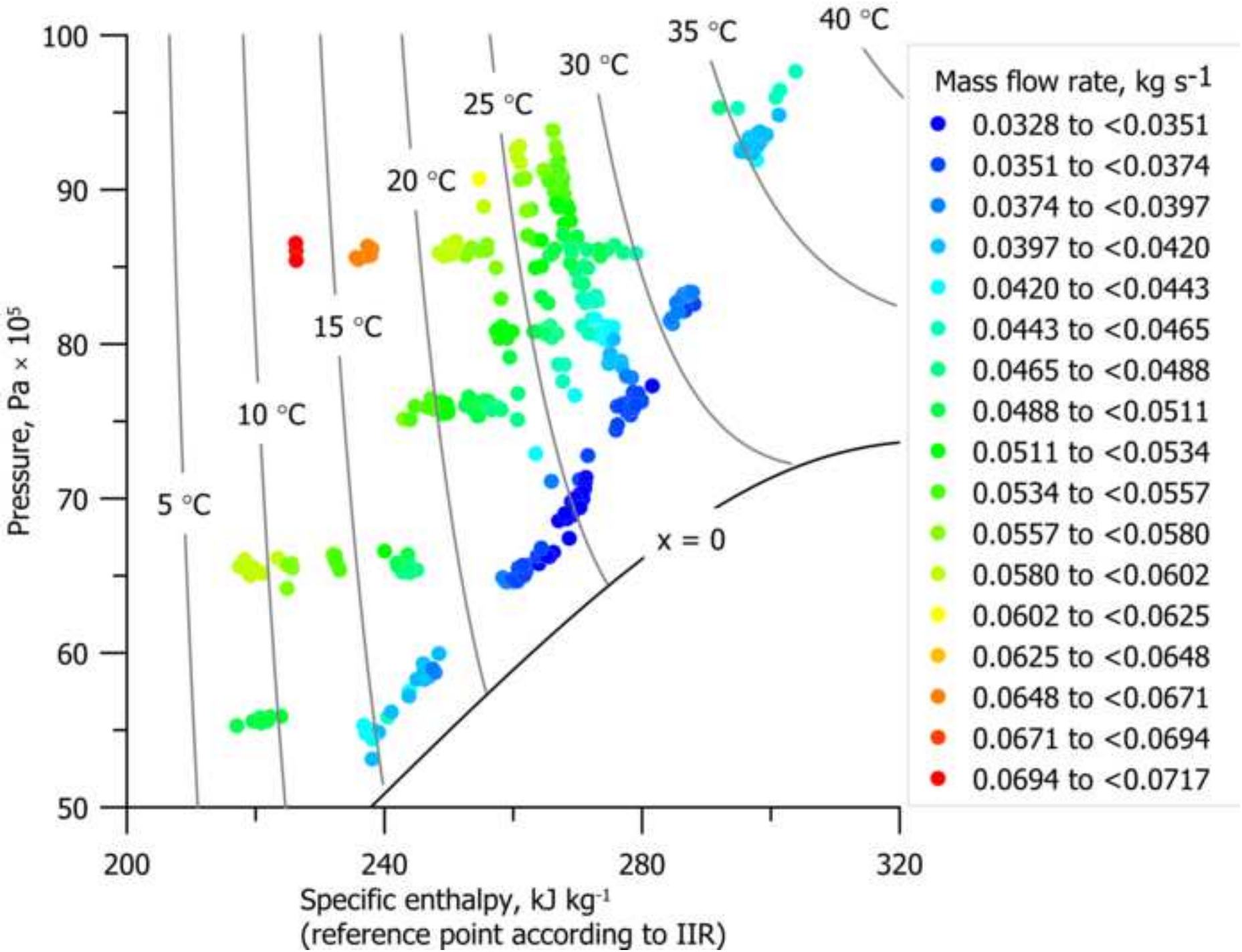

Figure_3b

Click here to download high resolution image

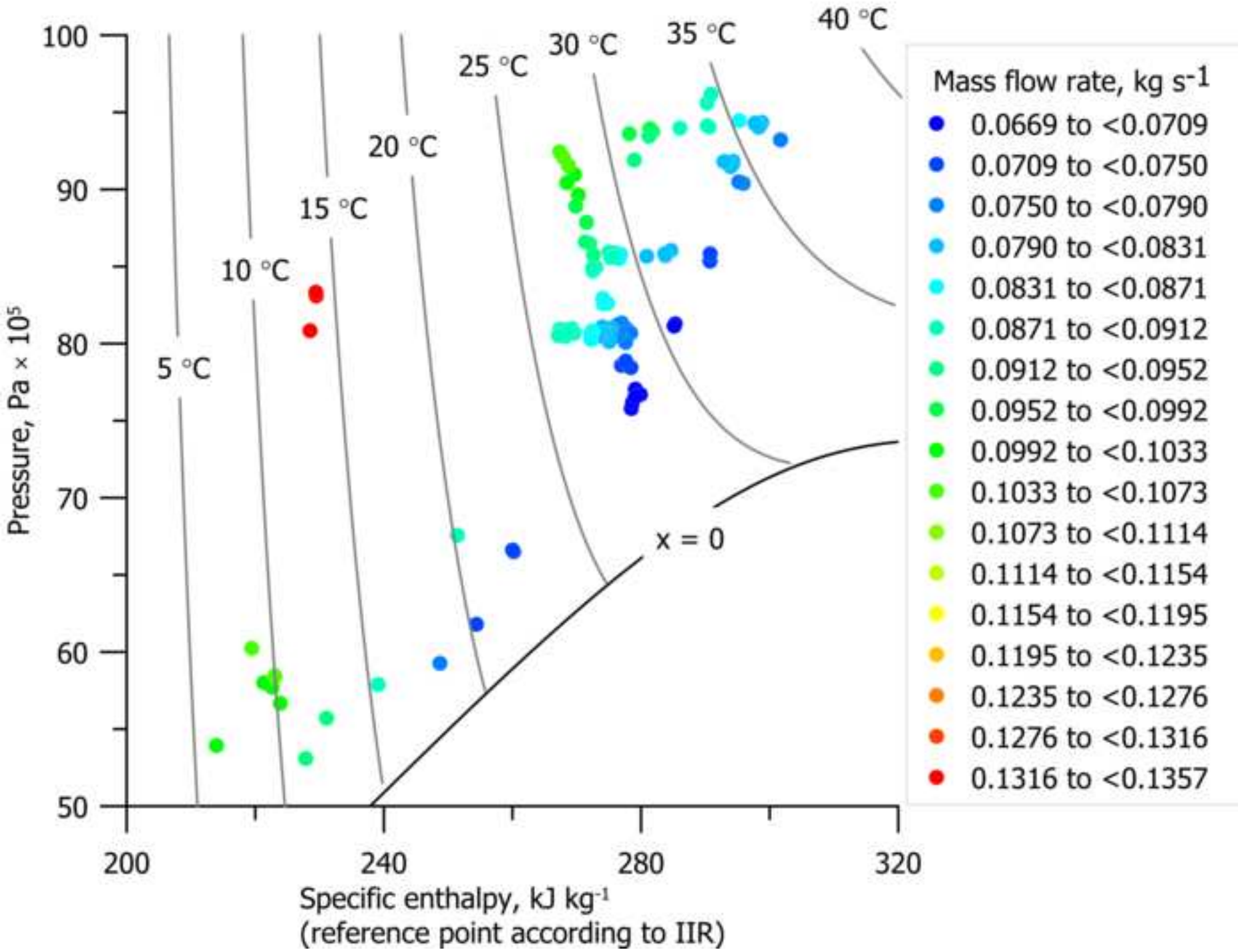

Figure_3c

Click here to download high resolution image

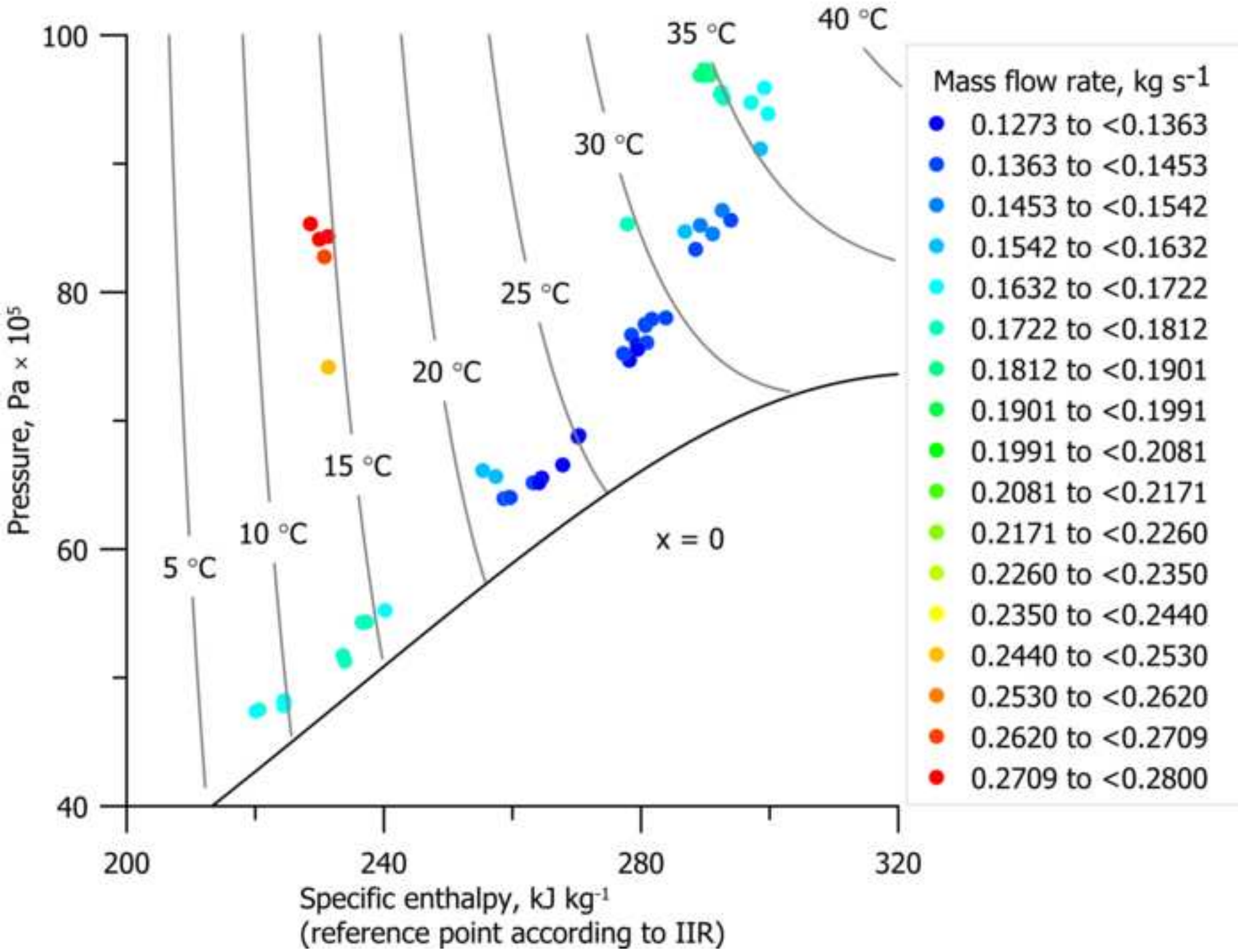

Figure_3d

Click here to download high resolution image

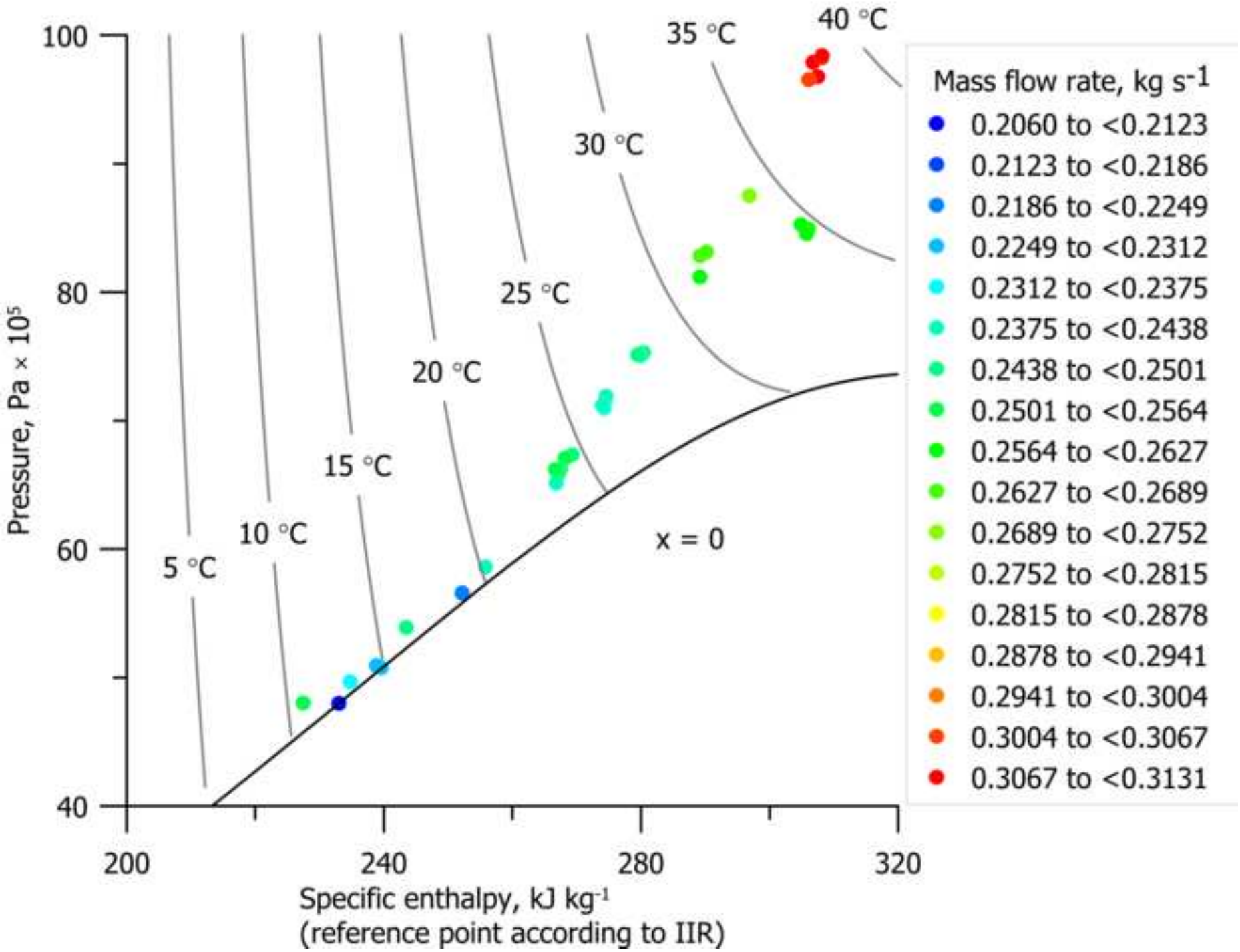

Figure_4
Click here to download high resolution image

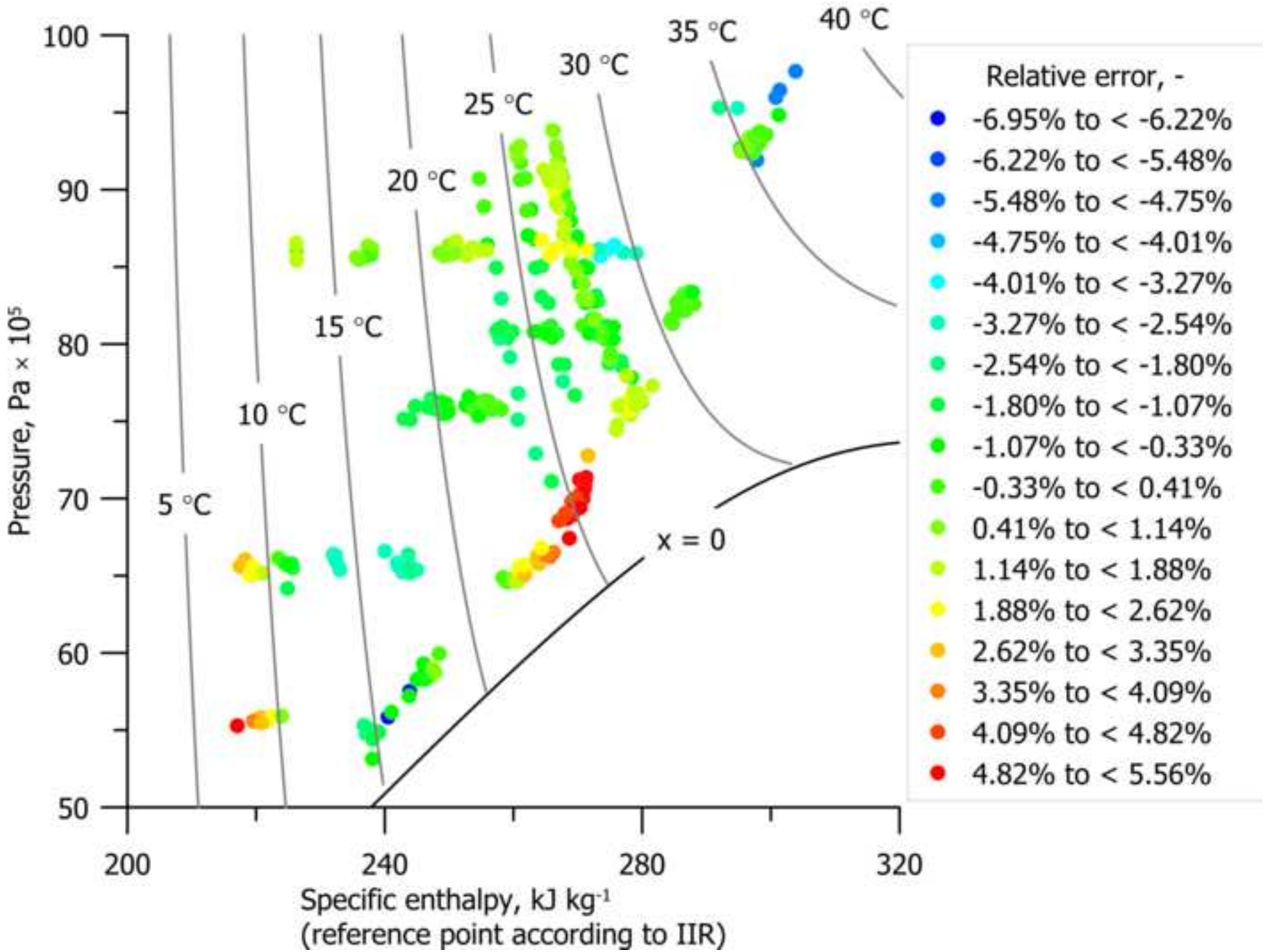

Figure_5a

Click here to download high resolution image

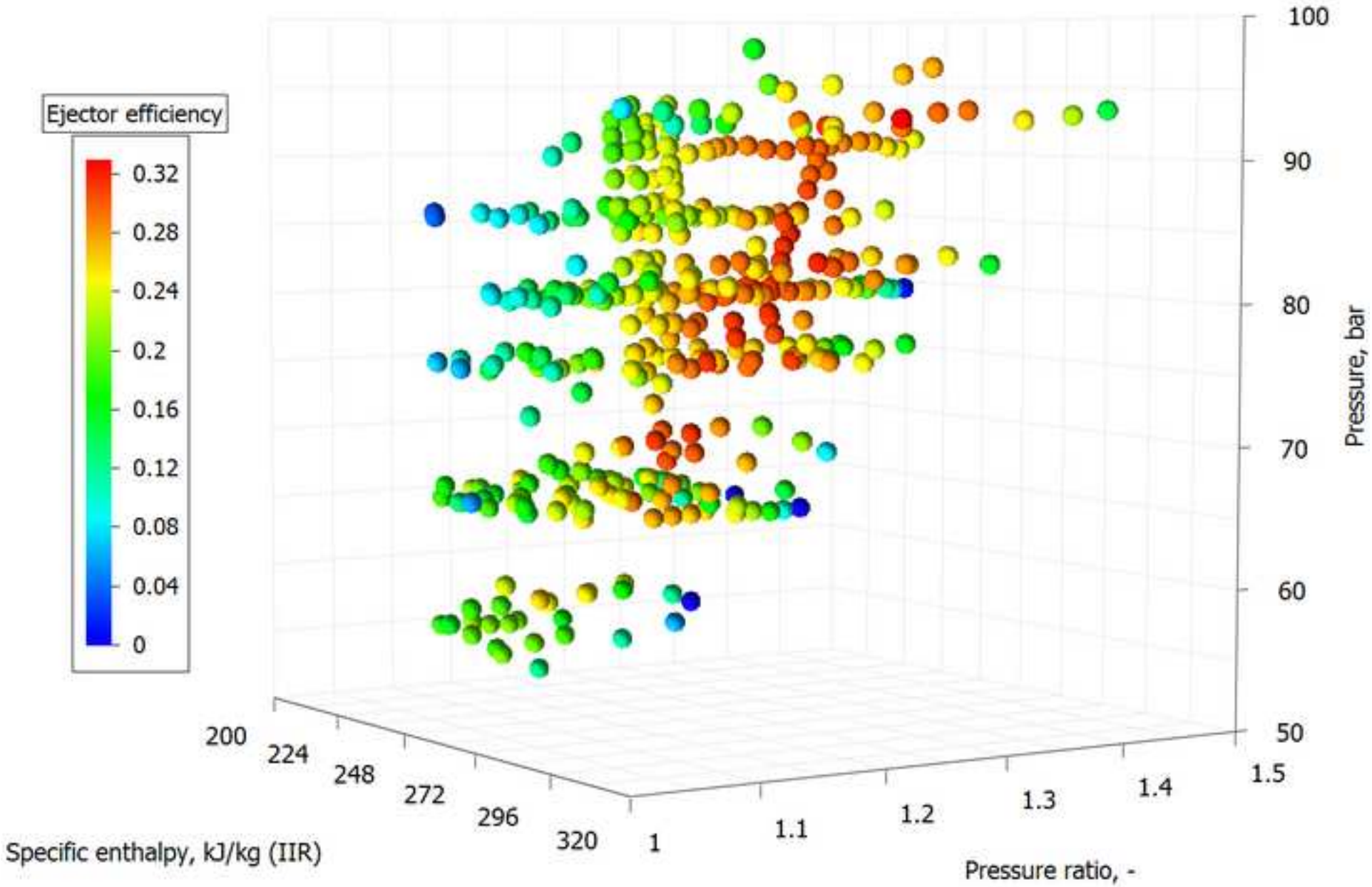

Figure_5b

Click here to download high resolution image

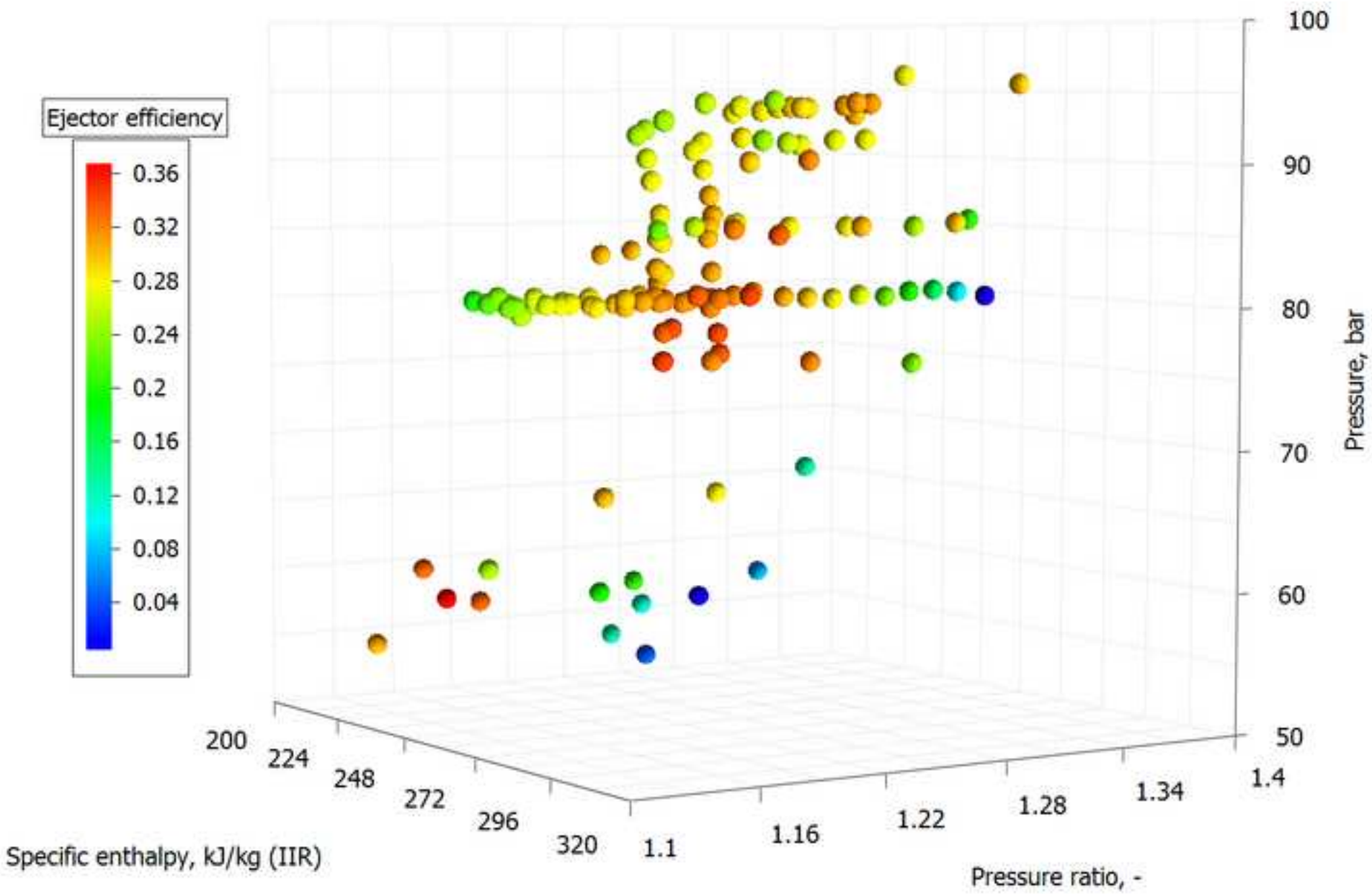

Figure_5c

Click here to download high resolution image

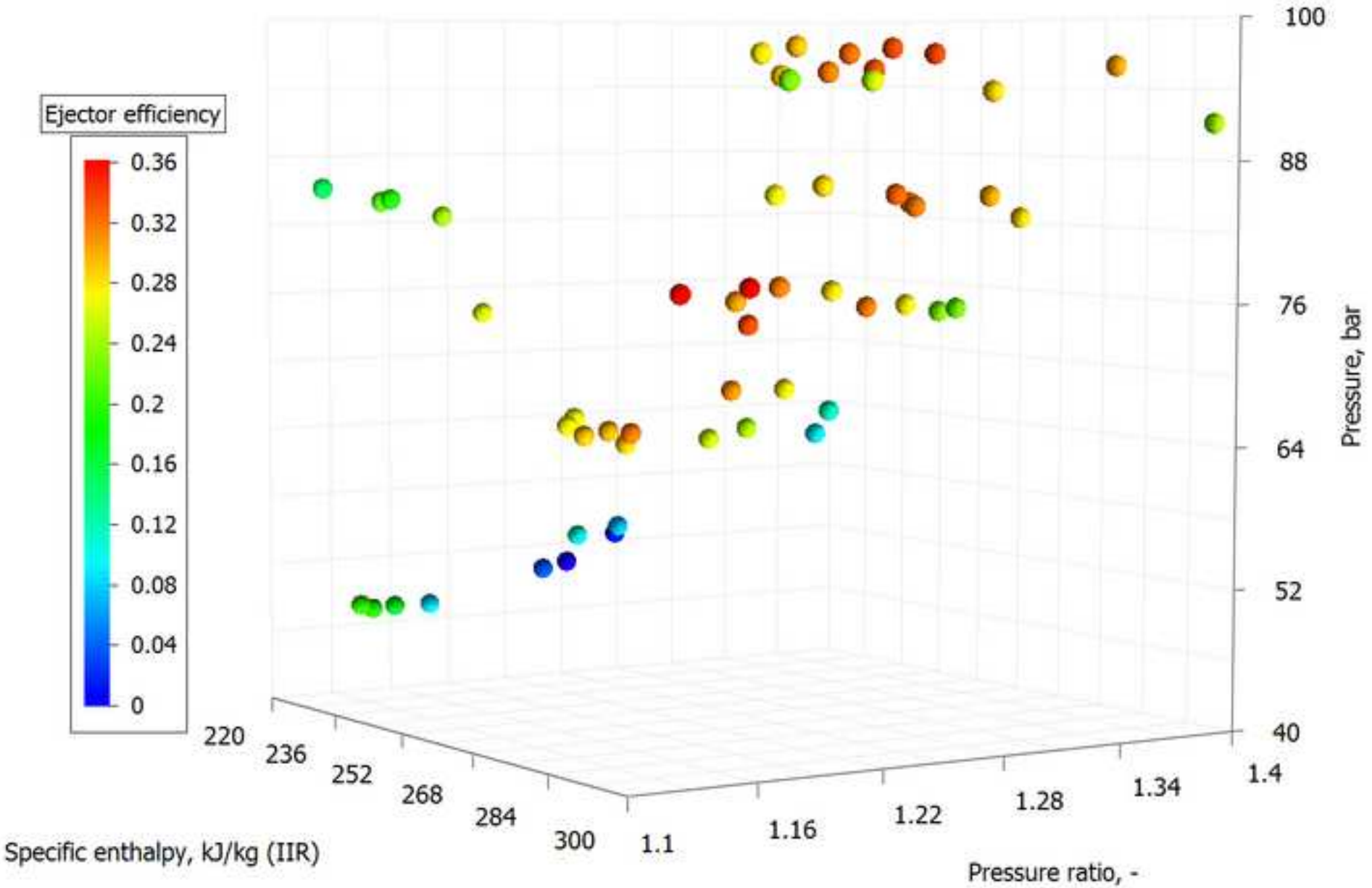

Figure_5d

Click here to download high resolution image

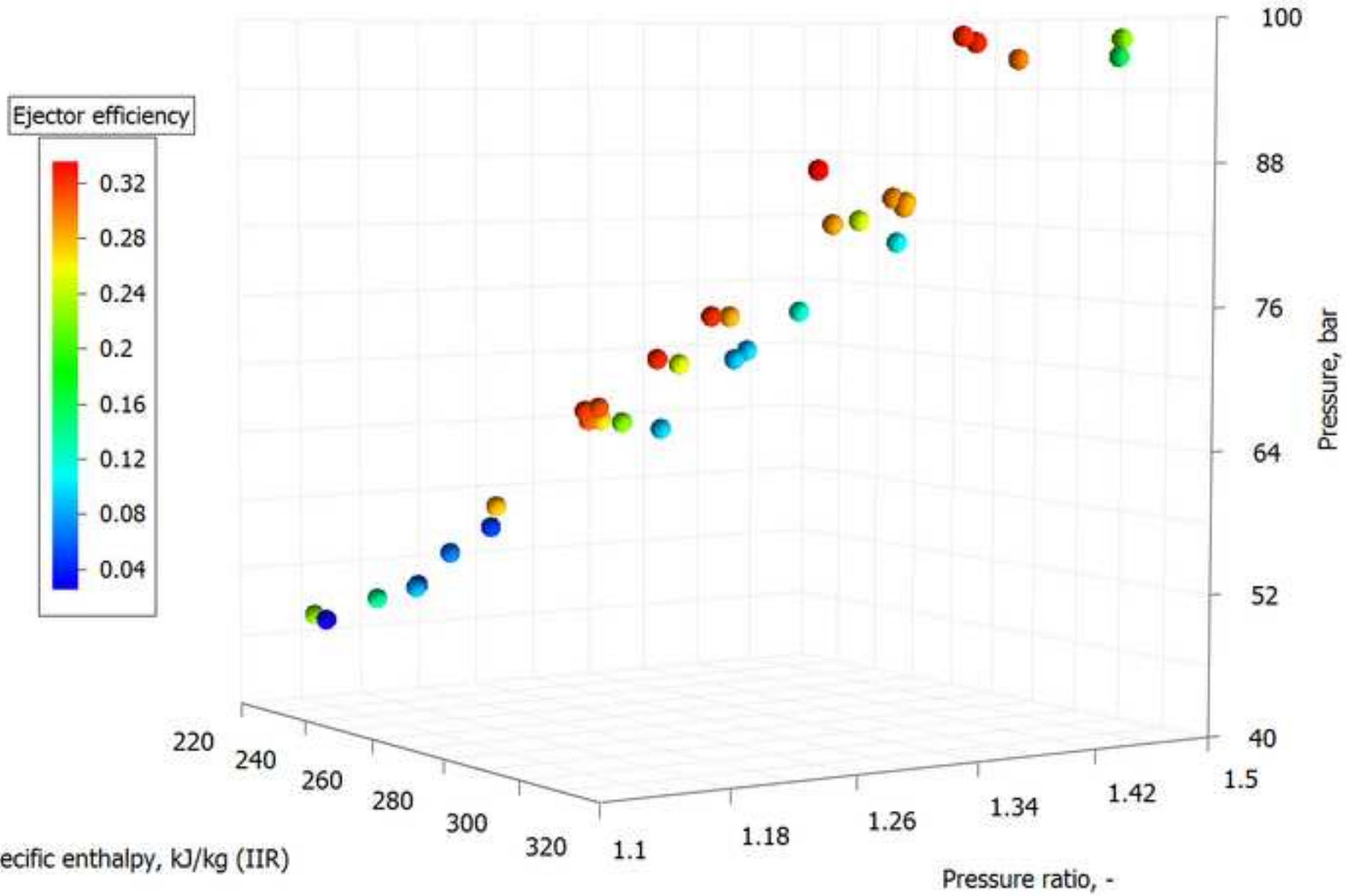

Figure_6
Click here to download high resolution image

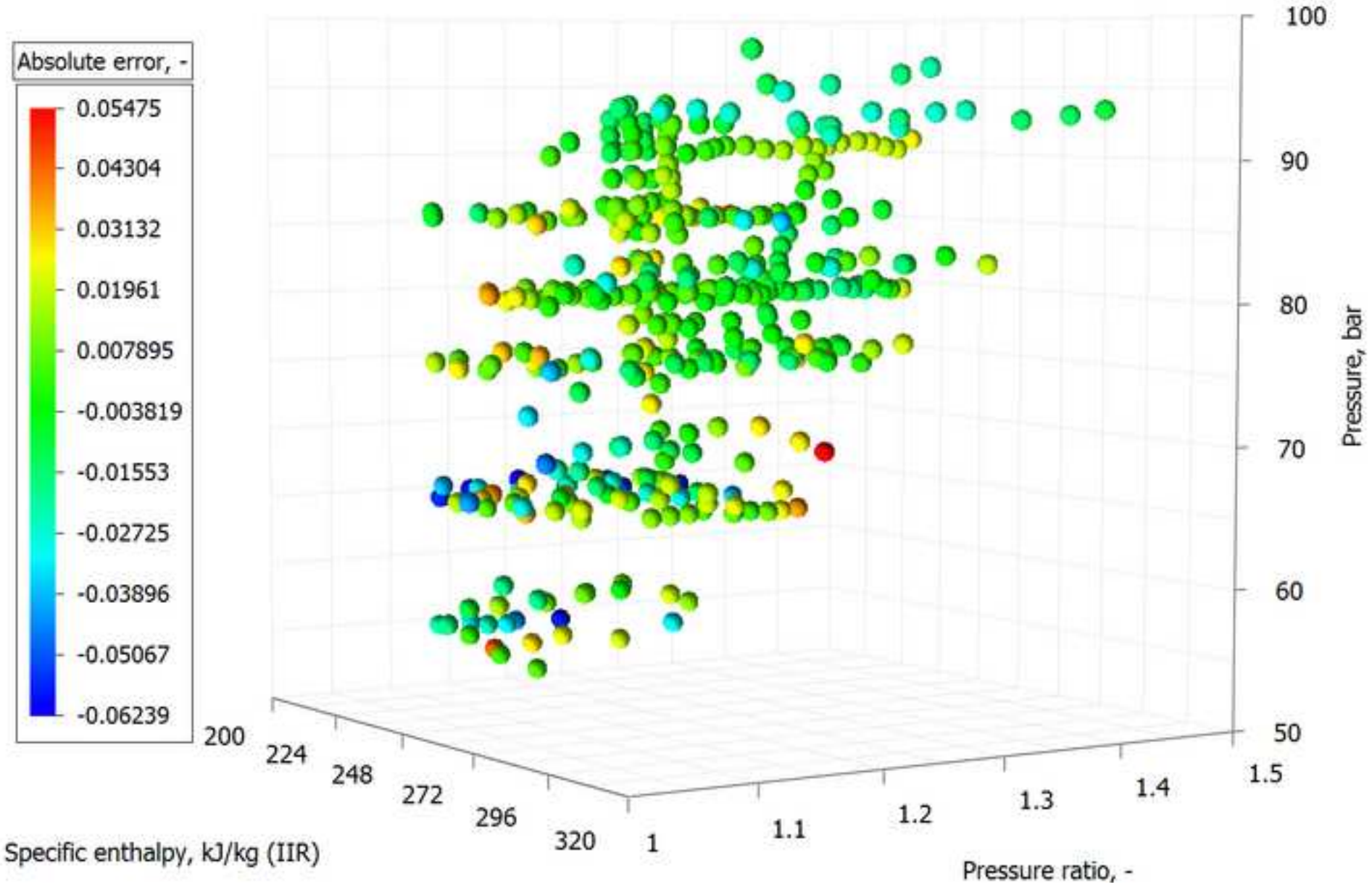

Figure_7
Click here to download high resolution image

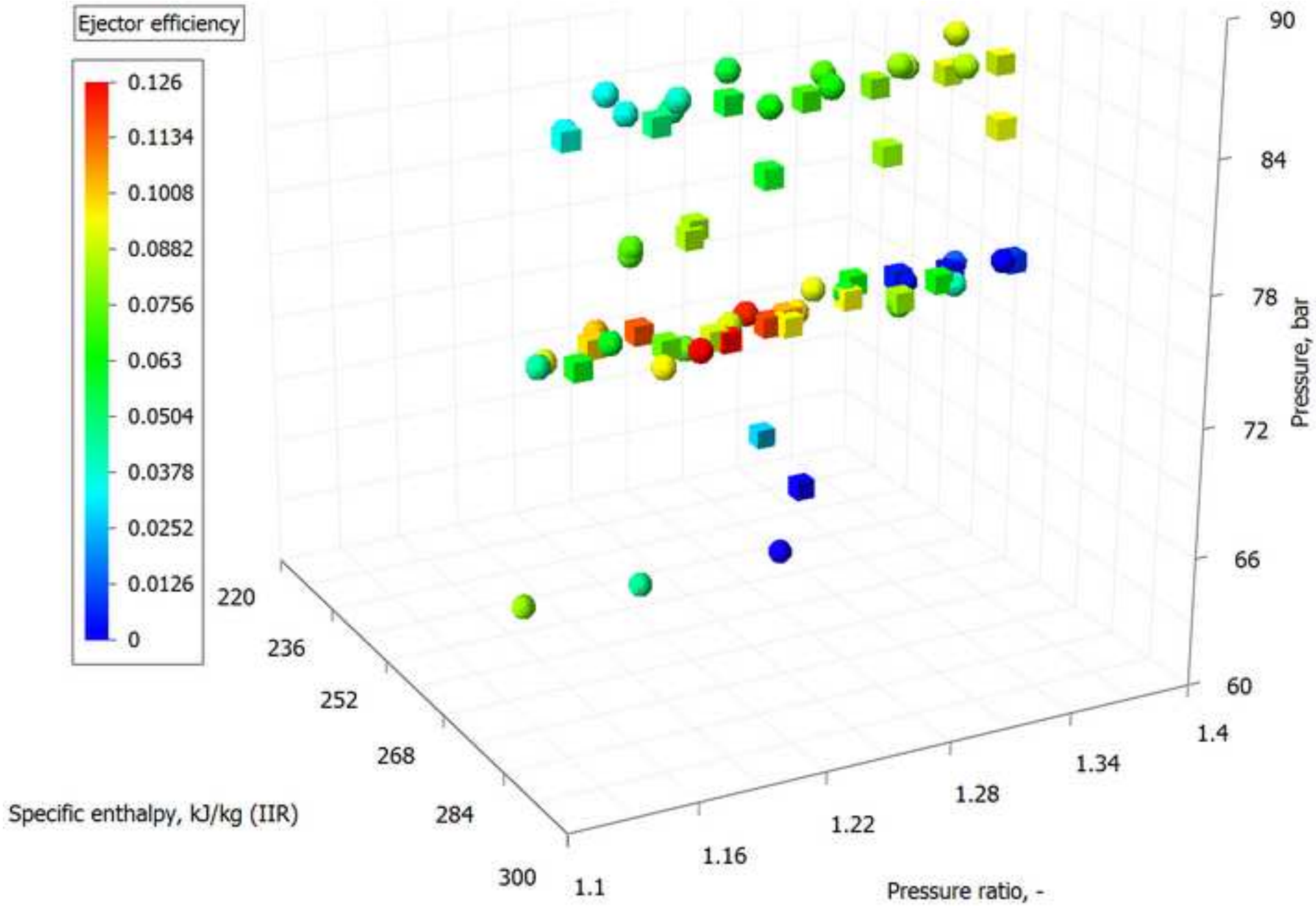

Figure_8

Click here to download high resolution image

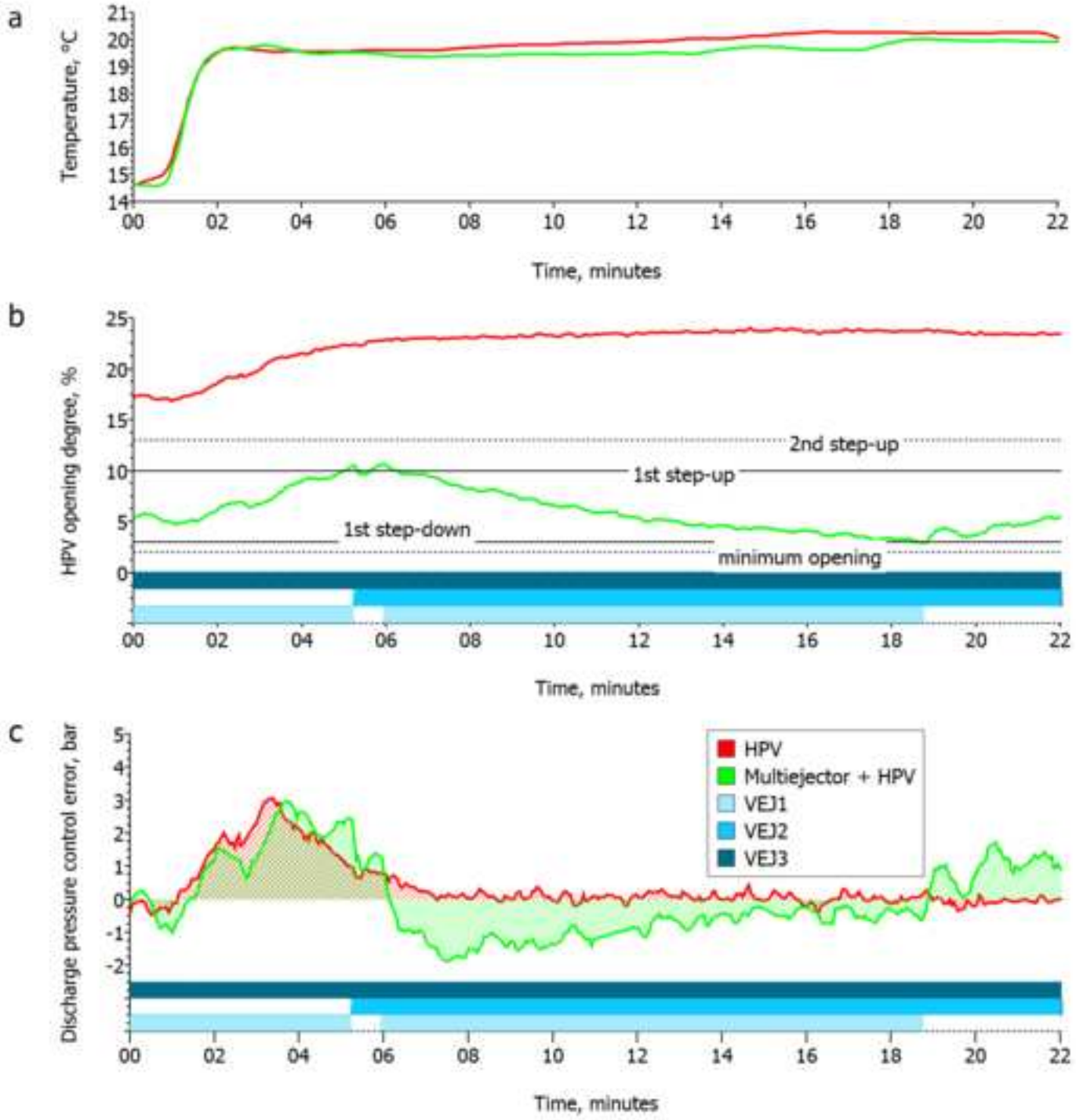

Figure_9
Click here to download high resolution image